J. Fluid Mech. (2003), *vol.* 497, *pp.* 335–363.
DOI: 10.1017/S0022112003006694 Printed in the United Kingdom

A hierarchy of low-dimensional models for the transient and post-transient cylinder wake

By BERND R. NOACK[1]†, KONSTANTIN AFANASIEV[2], MAREK MORZYŃSKI[3], GILEAD TADMOR[4] AND FRANK THIELE[1]

[1]Hermann-Föttinger-Institut für Strömungsmechanik, Technische Universität Berlin HF1, Straße des 17. Juni 135, D-10623 Berlin, Germany

[2]Konrad-Zuse-Zentrum für Informationstechnik Berlin (ZIB), Division Scientific Computing, Department Scientific Software, Takustr. 7, D-14195 Berlin-Dahlem, Germany

[3]Institute of Combustion Engines and Basics of Machine Design, Poznań University of Technology, ul. Piotrowo 3, PL 60-965 Poznań, Poland

[4]Department of Electrical and Computer Engineering, Northeastern University, 440 Dana Research Building, Boston, MA 02115, USA

(Received 20 February 2003 and in revised form 23 July 2003)

A hierarchy of low-dimensional Galerkin models is proposed for the viscous, incompressible flow around a circular cylinder building on the pioneering works of Stuart (1958), Deane *et al.* (1991), and Ma & Karniadakis (2002). The empirical Galerkin model is based on an eight-dimensional Karhunen–Loève decomposition of a numerical simulation and incorporates a new 'shift-mode' representing the mean-field correction. The inclusion of the shift-mode significantly improves the resolution of the transient dynamics from the onset of vortex shedding to the periodic von Kármán vortex street. In addition, the Reynolds-number dependence of the flow can be described with good accuracy. The inclusion of stability eigenmodes further enhances the accuracy of fluctuation dynamics. Mathematical and physical system reduction approaches lead to invariant-manifold and to mean-field models, respectively. The corresponding two-dimensional dynamical systems are further reduced to the Landau amplitude equation.

1. Introduction

In the current study, low-dimensional models are developed for the example of a cylinder wake. Low-dimensional modelling of incompressible flows plays an increasingly important role in academic and industrial research. Reduced flow models are a good test-bed for the understanding of the key physical processes, allow quick exploratory actuation studies, and enable the application of methods of control and dynamical systems theory. Thus, these coherent-structure descriptions fill the gap in the theoretical spectrum between analytical theory and high-dimensional accurate simulations. The mathematical foundation of many low-dimensional models was laid

† Author to whom correspondence should be addressed: NoackBR@pi.tu-berlin.de

about a hundred years ago with Galerkin models (see for example Holmes, Lumley & Berkooz 1998) and vortex methods (see for example Cottet & Koumoutsakos 2000).

The flow around a circular cylinder has been under active investigation for more than one hundred years. This configuration represents a paradigm of wakes as one of the major flow categories. Despite its simple geometry, the flow exhibits a rich kaleidoscope of phenomena (see for example Williamson 1996; Noack 1999*a*, *b*) and has served as a benchmark problem for many fluid-dynamics methods. In the present study, focus is placed on the two-dimensional, laminar flow with periodic vortex shedding.

Low-dimensional vortex models have successfully described qualitative properties of the cylinder wake, such as the steady solution by Föppl (1913) and its stabilization by Tang & Aubry (2000). Galerkin methods are the natural candidate to describe the globally synchronized dynamics, like the vortex shedding in the near wake (Rempfer 2003). The dimension and properties of the resulting Galerkin model strongly depend on the choice of the expansion modes in the Galerkin approximation. The approximation may be classified in terms of mathematical, physical, and empirical approaches.

Mathematical modes are derived as a complete countable set of orthonormal fields in a suitable Hilbert space. These modes fulfil the incompressibility condition and the boundary condition. The dimension of Galerkin systems with reasonable quantitative accuracy is easily of the order of hundreds (Noack & Eckelmann 1994*a*, *b*) for the laminar and transitional regime or even up to a thousand (Zebib 1987) for a more accurate resolution. Practically all mathematical Galerkin models are based on the carrier-field ansatz with two generalized stream functions and are hence restricted to simple geometries with nominally one- or two-dimensional boundary conditions.

Physical modes also satisfy some Navier–Stokes related eigenvalue problems. Examples are Stokes modes (Rummler 2000), singular Stokes modes (Batcho 1994; Kevrekidis *et al.* 1997) and eigenmodes of the linearized Navier–Stokes equations (Jackson 1987; Zebib 1987; Morzyński, Afanasiev & Thiele 1999). This leads to the hope of a reduction of the system dimension by incorporating some properties of the Navier–Stokes equation. This approach has proven successful for construction of low-dimensional models of internal flows (Rummler 2000). However, our experience with the wake flow is not very encouraging (Afanasiev 2003).

Empirical modes can be derived from a reference Navier–Stokes solution in an arbitrarily complex domain. The Karhunen–Loève decomposition is the most prominent example (see for example Holmes *et al.* 1998). In a pioneering study, Deane *et al.* (1991) have reproduced the dynamics of the laminar cylinder wake with a mere eight-dimensional empirical Galerkin model. In another landmark work by Ma & Karniadakis (2002), these models have been generalized to three-dimensional transition. Indeed, empirical Galerkin models provide very efficient representations of the reference dynamics, mostly with higher accuracy than mathematical and physical Galerkin models while employing fewer modes.

The price of this low-dimensionality is a lack of robustness away from the reference simulation, e.g. the restriction to a narrow range of Reynolds numbers. Deane *et al.* (1991) note that 'the accuracy of the model predictions rapidly deteriorate as we move away from the decomposition value'. In contrast, the mathematical Galerkin model by Noack & Eckelmann (1994*a*) describes the complete C-mode transition scenario (Karniadakis & Triantafyllou 1992; Zhang *et al.* 1995) from Reynolds numbers between one and 300. The maximum accuracy of the mathematical approach is not comparable with empirical models near the reference conditions. The mathematical

model also incorporates actuation effects, like cylinder rotation and translation (Hu *et al.* 1996). Alternatively, Afanasiev & Hinze (2001) employ an empirical Galerkin model for optimal complete-information control of the cylinder wake with a volume force. Here, the optimal actuation is determined from the low-dimensional Galerkin model based on the Karhunen–Loève decomposition of an actuated simulation in an iteration procedure.

The goal of the present study is to combine the strengths of empirical and mathematical Galerkin models with a hybrid approach. The proposed generalized Galerkin model exploits the excellent accuracy of the empirical approach for the reference condition and enhances the range of applicability and robustness due to ingredients of mathematical Galerkin models. The robustness is found to play an important role in system-reduction approaches, in the model-based prediction of actuation effects, and in controller design (Gerhard *et al.* 2003). In a similar spirit, another hybrid Galerkin model from empirical and physical modes has been developed for flexible walls (Rempfer *et al.* 2003).

The manuscript is organized as follows. A challenge arising from empirical Galerkin methods is exemplified by a model system in § 2. This consideration motivates a hierarchy of generalized empirical Galerkin models in § 3. Generalized and reduced Galerkin models of the cylinder wake are then described in § 4 and § 5, respectively. Finally, the main findings and their implications for other flows are outlined in § 6.

2. A challenge arising from empirical Galerkin methods

In this section, a generalization of the empirical Galerkin method and some system-reduction approaches are motivated by considering a three-dimensional system of ordinary differential equations. In § 2.1, this dynamical system is described. In § 2.2, the standard empirical Galerkin method based on Karhunen–Loève modes is shown to yield a structurally unstable Galerkin system. In § 2.3, the amplitude-selection mechanism is discussed. The last subsection concludes with a suggested generalization of the Galerkin method which is pursued for periodic wake flows.

2.1. *Model system*

By construction, the empirical Galerkin model approximately accommodates the attractor provided that the residual of the Galerkin approximation is small enough. In this case, the solution is expected to stay close to the true attractor for some period of time. However, arbitrarily small perturbations of the Galerkin model may lead to large deviations of the Galerkin solution from the Navier–Stokes solution. To illustrate this possibility, a three-dimensional model system is considered,

$$\frac{\mathrm{d}}{\mathrm{d}t}u = \mu u - v - uw, \tag{2.1a}$$

$$\frac{\mathrm{d}}{\mathrm{d}t}v = \mu v + u - vw, \tag{2.1b}$$

$$\frac{\mathrm{d}}{\mathrm{d}t}w = -w + u^2 + v^2. \tag{2.1c}$$

Throughout this section, $\mu = 1/10$.

The model system has an unstable fixed point at the origin $\boldsymbol{u}_s := (u_s, v_s, w_s) = \boldsymbol{0}$ and a stable periodic solution which defines a limit cycle of radius $\sqrt{\mu}$ in the $w = \mu$ plane,

$$u = \sqrt{\mu}\,\cos t, \quad v = \sqrt{\mu}\,\sin t, \quad w = \mu. \tag{2.2}$$

This limit cycle is asymptotically and globally stable. Thus, the system has similar dynamics to the laminar periodic flow around a circular cylinder with an unstable steady solution and stable periodic vortex shedding. Moreover, the system has a quadratic nonlinearity, like the Navier–Stokes equation.

2.2. *Structural instability of the empirical Galerkin system*

The Karhunen–Loève decomposition of the periodic solution (2.2) leads to

$$\boldsymbol{u}^{[2]} := \boldsymbol{u}_0 + a_1\boldsymbol{u}_1 + a_2\boldsymbol{u}_2, \tag{2.3}$$

with the average value $\boldsymbol{u}_0 := (0, 0, \mu)$, as a counterpart of the mean flow, and the Karhunen–Loève modes $\boldsymbol{u}_1 := (1, 0, 0)$, $\boldsymbol{u}_2 := (0, 1, 0)$. The Galerkin approximation (2.3) describes the solution (2.2) exactly with the Fourier coefficients $a_1 = \sqrt{\mu}\,\cos t$, $a_2 = \sqrt{\mu}\sin t$, and spans only the two-dimensional plane $w = \mu$ within the entire, three-dimensional state space. For later reference, this plane shall be called the *Karhunen–Loève space*. The loss of state-space dimensions (here, a drop by one dimension) is associated with unresolved eigenvectors of vanishing empirical eigenvalues (see for instance Holmes *et al.* 1998).

In a Galerkin projection, (2.3) is substituted in the model system (2.1) and projected on $\boldsymbol{u}_1$, $\boldsymbol{u}_2$ using the standard Euclidean inner product. The resulting equation describes a marginally stable centre around $(a_1, a_2) = (0, 0)$ without preference for any amplitude,

$$\frac{\mathrm{d}}{\mathrm{d}t}a_1 = -a_2, \quad \frac{\mathrm{d}}{\mathrm{d}t}a_2 = a_1. \tag{2.4}$$

Evidently, an arbitrarily small perturbation of the autonomous system, such as $\mathrm{d}a_1/\mathrm{d}t = \epsilon a_1 - a_2$, $\mathrm{d}a_2/\mathrm{d}t = \epsilon a_2 + a_1$, may give rise to exploding, vanishing, or otherwise incorrect solutions of the system. Hence, the Galerkin system (2.4) is *structurally unstable* (see for instance the definition in Guckenheimer & Holmes 1986, § 1.7).

In the above example, the Galerkin approximation is exactly valid but the resulting empirical Galerkin model has, nevertheless, incorrect attractors. A similar result has been obtained by Rempfer (2000) in another dynamical system. Here, the empirical Galerkin method even gives rise to an unstable Galerkin attractor – in contrast to the stable attractor of the original system.

2.3. *Amplitude-selection mechanism*

The two-dimensional Galerkin model (2.4) conserves the initial amplitude $A = \sqrt{x^2 + y^2}$ and fails to predict any transient. In the original system, the transient trajectory quickly approaches the manifold $w = u^2 + v^2$ and spirals outwards on the paraboloid. Figure 1 displays such a trajectory which starts in the plane of the limit cycle at (0.001, 0, 0.1). Evidently, the Karhunen–Loève decomposition (2.3) does not resolve the third dimension in the model (2.1). This third phase-space direction is spanned by the mean-field correction, i.e. the difference between the averaged attractor $(0, 0, \mu)$ and the steady solution $\mathbf{0}$.

The mean-field correction plays a major role in the transient dynamics. This role can be assessed by re-writing the model system (2.1) in the form

$$\frac{\mathrm{d}}{\mathrm{d}t}u = \sigma_w u - v, \tag{2.5a}$$

$$\frac{\mathrm{d}}{\mathrm{d}t}v = \sigma_w v + u, \tag{2.5b}$$

$$\frac{\mathrm{d}}{\mathrm{d}t}w = -w + u^2 + v^2, \tag{2.5c}$$

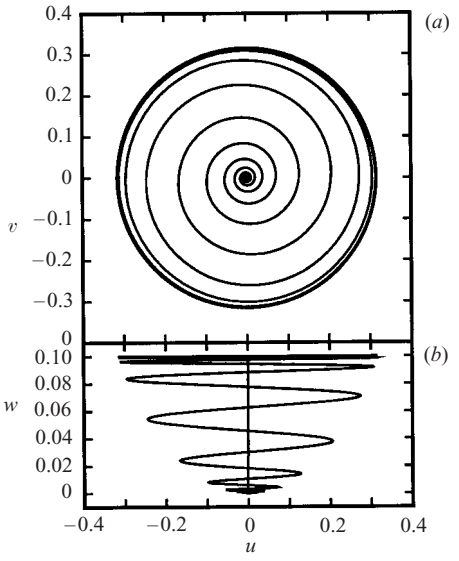

FIGURE 1. Solution of the model problem (2.1) starting from the initial condition (0.001, 0, 0.1). The figure displays the u, v- (a) and the u, w-phase portraits (b) of the trajectory.

where $\sigma_w := \mu - w$ can be interpreted as a growth rate of the oscillation amplitude $A := \sqrt{u^2 + w^2}$ in the plane $w = \text{const}$. This interpretation is corroborated by re-writing (2.5) in cylindrical coordinates using $\phi = \arctan(v/u)$,

$$\frac{\mathrm{d}}{\mathrm{d}t}A = \sigma_w A, \tag{2.6a}$$

$$\frac{\mathrm{d}}{\mathrm{d}t}\phi = 1, \tag{2.6b}$$

$$\frac{\mathrm{d}}{\mathrm{d}t}w = -w + A^2. \tag{2.6c}$$

The oscillation amplitude increases 'below' the limit cycle $w < \mu$, since $\sigma_w > 0$, and decreases above the limit cycle (see figure 2). The growth rate σ_w characterizes the dynamics in every two-dimensional plane of the phase space with a 'frozen' w. Figure 3 displays these cuts containing the fixed point, the limit cycle and a point in the stable regime.

The limit cycle is determined by $\mathrm{d}A/\mathrm{d}t = \mathrm{d}w/\mathrm{d}t = 0$, or, equivalently, by $\sigma_w = \mu - w = 0$ and $w = A^2$. The latter equation defines a paraboloid in phase space. The paraboloid plays an important role not only for the limit cycle but also for the transients. The numerical solutions in figures 1 and 2 quickly approach this paraboloid. This behaviour can be derived from (2.6) using a small-parameter argument. The growth rate associated with the oscillation amplitude is $\sigma_w := \mu - w$. For a transient from the fixed point to the limit cycle, this growth rate is in the interval $0 \leqslant \sigma_w \leqslant 0.1$, i.e. it is 'small' and positive. In contrast, the linearized dynamics of the w-direction are described by $\mathrm{d}w/\mathrm{d}t = -w$, i.e. the w-direction is stable and has a time scale which is at least one order of magnitude smaller than the time scale of the oscillation-amplitude dynamics. Hence, the slaving principle (see for instance Haken 1983) suggests replacing the differential equation (2.6c) by an algebraic equation derived

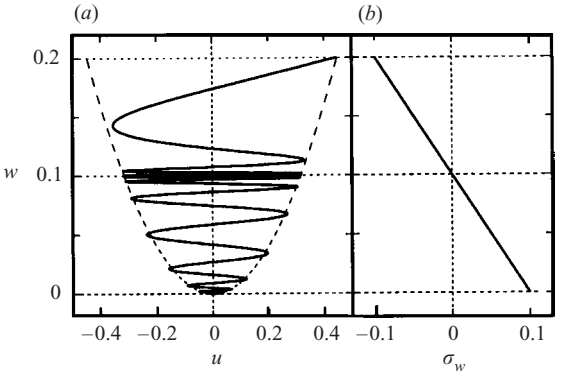

FIGURE 2. Solutions of the model system (a) and growth rate σ_w as functions of w (b). In (a) the u, w-phase portrait of two transient solutions approaching the limit cycle from initial conditions $\boldsymbol{u} = (\sqrt{0.2}, 0, 0.2)$ and $\boldsymbol{u} = (0.001, 0, 0)$ is displayed.

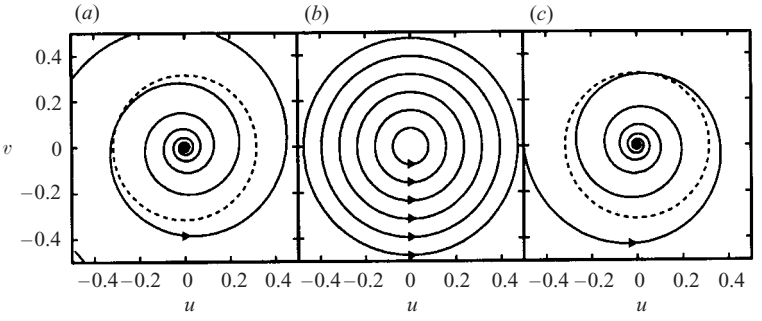

FIGURE 3. Solutions of the two-dimensional model system (2.1a, b) in the (u, v)-plane with the third coordinate frozen at (a) $w = 0$, (b) $w = \mu$, and (c) $w = 2\mu$.

from $\mathrm{d}w/\mathrm{d}t = 0$. Thus,

$$\frac{\mathrm{d}}{\mathrm{d}t}A = \sigma_w A, \quad w = +A^2. \tag{2.7}$$

The paraboloid $w = A^2$ is also a second-order centre-manifold expansion around $\boldsymbol{u} = 0$ and $\mu = 0$ (see for instance Copeland & Noack 2000). In addition, the restriction of the dynamics to the paraboloid can also be derived from mean-field theory (see for instance Noack & Copeland 2000).

The nonlinear dynamics of the oscillation amplitude are derived from (2.7) by eliminating w. This elimination leads to the well-known Landau equation,

$$\frac{\mathrm{d}}{\mathrm{d}t}A = \mu A - A^3. \tag{2.8}$$

It is important to note that the amplitude-selection mechanism described by the Landau equation cannot be obtained within the marginally stable Karhunen–Loève space, but is closely linked to the paraboloid. The marginal stability of the averaged model solution has also been theoretically conjectured and numerically shown for a large class of laminar and turbulent shear flow (Noack & Bertolotti 2000).

The model system exemplifies both a challenge and an enhancement of the empirical Galerkin method. The challenge rests in the well-known fact that possibly important

phase directions are not resolved in the Karhunen–Loève decomposition of the post-transient flow. As a remedy to this situation, the model system suggests including the mean-field direction in a generalized Karhunen–Loève decomposition. This ansatz is pursued in the next section for the wake flow.

3. Hierarchy of generalized Galerkin models

In this section, a hierarchy of flow models is proposed. This hierarchy ranges from a direct numerical simulation to an amplitude equation. In § 3.1, the flow configuration and direct numerical simulation are described. In § 3.2, the generalized Galerkin model is proposed. Mathematical and physical system-reduction approaches are described in § 3.3 and § 3.4, respectively. These reduced-order models enable the derivation of an amplitude equation for transient dynamics.

3.1. *Navier–Stokes simulation*

In this subsection, the initial boundary value problem for the incompressible flow is formulated and the corresponding Navier–Stokes solver is outlined.

The two-dimensional flow is described in a Cartesian coordinate system, x, y, where the x-axis is aligned which has oncoming flow and the y-axis is perpendicular to this direction. The origin is in the centre of the cylinder which has diameter D. Location is denoted by a vector $\boldsymbol{x}=(x, y)$, and time by t. The velocity vector is $\boldsymbol{u} = (u, v)$, where u and v are the components in the x- and y-direction, respectively. Pressure is denoted by p. In the following, all variables are assumed to be non-dimensionalized with respect to the cylinder diameter D and the oncoming flow U.

The evolution of the flow is described by the incompressibility condition and the Navier–Stokes equation,

$$\nabla \cdot \boldsymbol{u} = 0, \tag{3.1a}$$

$$\partial_t \boldsymbol{u} + \nabla \cdot (\boldsymbol{u}\,\boldsymbol{u}) = -\nabla p + \frac{1}{Re}\Delta \boldsymbol{u}, \tag{3.1b}$$

where $Re = UD/\nu$ represents the Reynolds number with kinematic viscosity ν. The standard notation of tensor algebra is employed for multiplication and for differentiation, e.g. $\boldsymbol{u}\,\mathbf{v}$ denotes the outer product between the vectors $\boldsymbol{u}$, $\boldsymbol{v}$ leading to a matrix, '$\cdot$' is a single contraction, ∇ denotes the Nabla operator, and Δ represents the Laplace operator.

The computational domain Ω for the flow is the exterior of the cylinder $x^2 + y^2 \geqslant (1/2)^2$ in the rectangle $-5 \leqslant x \leqslant 15$, $-5 \leqslant y \leqslant 5$. The boundary condition consists of a no-slip condition at the cylinder, a uniform free-stream condition at the inflow $u = 1$, $v = 0$, the same condition at the transverse boundaries, and a stress-free outflow condition $\boldsymbol{\sigma} \cdot \boldsymbol{n} = 0$ with the stress tensor $\sigma_{ij} = -p\delta_{ij} + Re^{-1}(\partial_j u_i + \partial_i u_j)$ and the outflow direction $\boldsymbol{n}$.

Targeting more complex geometries, the flow is discretized as finite elements on a triangular mesh. The corresponding grid is shown in figure 4. The finite-element Navier–Stokes solver is third-order accurate in space and time and based on a pseudo-pressure formulation (see for instance Fletcher 1988, § 17.2). The average lengths of the triangular mesh elements are 0.058 near the cylinder, 0.066 on the wake centreline $x > 0.5$, $y = 0$, and 0.104 in the whole domain. Each mesh element is subdivided in four similar subtriangles the vertices of which serve as nodes for the flow variables. The Navier–Stokes solver has been employed in numerous investigations including the

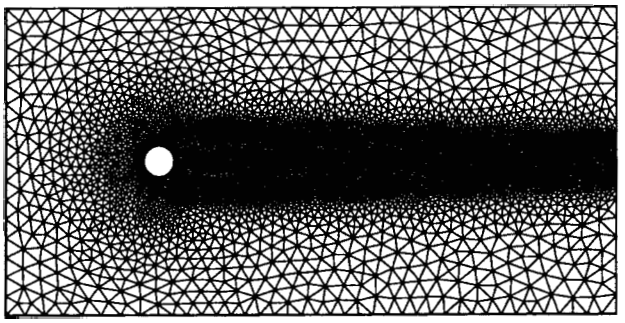

FIGURE 4. Computational grid in Ω.

flow around a circular cylinder. Details of the solver are provided in other references (Afanasiev 2003; Gerhard 2003; Morzyński 1987; and the references therein).

The chosen domain size and discretization order is, on the one hand, large enough for a good accuracy, and on the other hand, small enough to allow the computationally challenging global linear stability analysis which is performed on the same grid. The numerical computation of the Galerkin model has the same order of accuracy as the simulation.

3.2. *Generalized empirical Galerkin model*

In this section, a generalization of the empirical Galerkin method is proposed.

A standard empirical Galerkin model is based on a Karhunen–Loève expansion of the reference simulation (see for example Holmes *et al.* 1998). In this decomposition, the flow $\boldsymbol{u}$ is approximated by a finite Galerkin approximation $\boldsymbol{u}^{[N]}$,

$$\boldsymbol{u}(\boldsymbol{x}, t) \approx \boldsymbol{u}^{[N]} := \boldsymbol{u}_0(\boldsymbol{x}) + \sum_{i=1}^{N} a_i(t)\, \boldsymbol{u}_i(\boldsymbol{x}), \tag{3.2}$$

where $\boldsymbol{u}_0$ represents the mean flow, $\{\boldsymbol{u}_i\}_{i=1}^{N}$ the first N Karhunen–Loève modes, and a_i the time-dependent Fourier coefficients. The coefficients are expressed by

$$a_i = (\boldsymbol{u} - \boldsymbol{u}_0,\ \boldsymbol{u}_i)_\Omega,$$

where $(\boldsymbol{v}, \boldsymbol{w})_\Omega := \int_\Omega \mathrm{d}A\, \boldsymbol{v} \cdot \boldsymbol{w}$ represents the inner product between two solenoidal fields $\boldsymbol{v}, \boldsymbol{w}$ on the computational domain Ω. For later reference, the norm $\|\boldsymbol{v}\|_\Omega := \sqrt{(\boldsymbol{v}, \boldsymbol{v})_\Omega}$ is introduced.

In the current study, the Karhunen–Loève modes are computed with a snapshot method from about 100 snapshots of a periodic reference simulation at $Re = 100$. The snapshots are sampled uniformly in one period. Deane *et al.* (1991) observe that as few as 20 snapshots are sufficient for the construction of the first eight eigenmodes. Figure 5 displays the first eight Karhunen–Loève modes. The modes $\boldsymbol{u}_i$ with $i = 1, 2, 5, 6$ are anti-symmetric with respect to the x-axis,

$$u_i(x, -y) = -u_i(x, y), \tag{3.3a}$$
$$v_i(x, -y) = +v_i(x, y), \tag{3.3b}$$

whereas the remaining modes are symmetric,

$$u_i(x, -y) = +u_i(x, y), \tag{3.4a}$$
$$v_i(x, -y) = -v_i(x, y). \tag{3.4b}$$

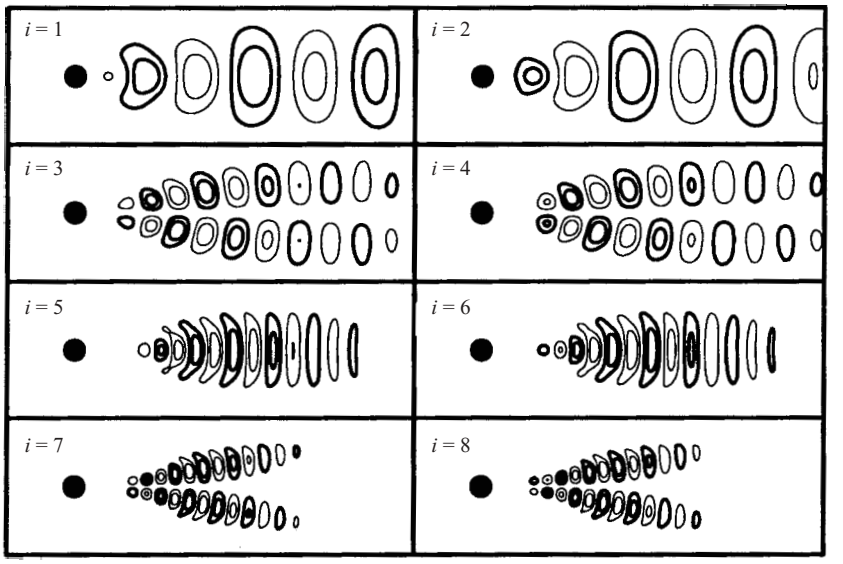

FIGURE 5. Karhunen–Loève decomposition at $Re = 100$. The flow field of the first eight Karhunen–Loève modes, $\boldsymbol{u}_i$, $i = 1, 2, \ldots, 8$, is visualized by iso-contour lines of the stream function. Positive (negative) values are indicated by thick (thin) lines. The cylinder is represented by the solid circle.

The mean flow and steady solution belong to the latter class. It should be noted that the velocity components u and v have opposite symmetry properties. The symmetry of the mode stated above refers only to its u-component — following a convention of linear stability analysis (see for instance Sato 1960).

The modes can be grouped as pairs $(\boldsymbol{u}_1, \boldsymbol{u}_2)$, $(\boldsymbol{u}_3, \boldsymbol{u}_4)$, $(\boldsymbol{u}_5, \boldsymbol{u}_6)$, $(\boldsymbol{u}_7, \boldsymbol{u}_8)$, etc. with alternating symmetry properties. Moreover, the nth pair approximately resolves the nth harmonics. This behaviour can be inferred from the Lissajous figures in earlier studies (Deane *et al.* 1991; Ma & Karniadakis 2002).

The energy in the ith Karhunen–Loève mode is quantified by the Karhunen–Loève eigenvalue

$$\lambda_i = \left\langle (\boldsymbol{u} - \boldsymbol{u}_0,\ \boldsymbol{u}_i)^2_\Omega \right\rangle = \left\langle a_i^2 \right\rangle, \tag{3.5}$$

where $\langle\,\rangle$ represents the time average of the quantity within, and $\lambda_i/2$ can be considered as the kinetic energy of the ith mode. Figure 6 displays the dominant part of the Karhunen–Loève spectrum at three Reynolds numbers. The two modes of each pair have similar energy, and the decay of energy from one pair to the next is approximately in a geometric progression. This behaviour is consistent with an asymptotic theory by Dušek, Le Gal & Fraunie (1994) and Dušek (1996). This theory predicts a nearly constant amplitude ratio between the $(n+1)$th and nth Fourier modes of a periodic flow.

The Karhunen–Loève decomposition (3.2) can be shown to be optimal for the reference simulation: the corresponding time-averaged energy residual is the smallest of all expansions with N modes (see for instance Holmes *et al.* 1998) and hence the Galerkin approximation (3.2) can be expected to be very efficient for the periodic flow.

However, this expansion does not resolve the steady solution. Evidently, the long steady vortex bubble (figure 7*a*) cannot be spanned by the time-averaged flow

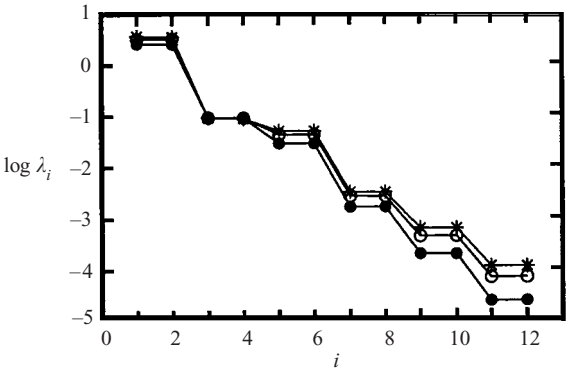

FIGURE 6. Karhunen–Loève eigenvalues. The symbols refer to the first eigenvalues λ_i in dependence of the mode number $i=1, 2, \ldots, 12$ at $Re=100$ (●), $Re=150$ (○) and $Re=200$ (⋆).

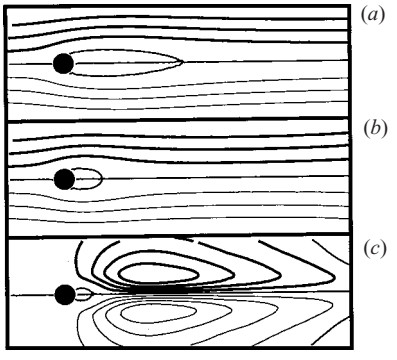

FIGURE 7. Construction of the shift-mode (c) from the steady solution (a) and the averaged flow (b) at $Re=100$. The flow field is visualized as in figure 5.

with a short bubble and the wave-like Karhunen–Loève modes. This restriction has important implications for the Galerkin model, as will be further elaborated in subsequent sections:

(i) the fixed point of the Galerkin model is the averaged flow $\boldsymbol{u}_0$ as opposed to the correct steady Navier–Stokes solution $\boldsymbol{u}_s$ (see § 4.3);

(ii) the predicted transient time from the fixed point to the limit cycle is much too long (see § 4.3);

(iii) the Galerkin model is predisposed to a structural instability (see § 2);

(iv) the Galerkin model exhibits a strong Re sensitivity (see Deane *et al.* 1991).

In other words, the price for the efficient low-dimensional description of the reference simulation is a low accuracy for transients and for a variation in the Reynolds number.

A natural extension of the Galerkin approximation for transient flow is the inclusion of an additional vector pointing from the steady Navier–Stokes solution $\boldsymbol{u}_s$ to the Karhunen–Loève space defined by (3.2). The steady solution is computed with a Newton iteration employing the discretized steady Navier–Stokes equation. The new phase-space direction is constructed in the following Gram–Schmidt procedure

starting from the mean-field correction $\boldsymbol{u}_0 - \boldsymbol{u}_s$:

$$\boldsymbol{u}_\Delta^a := \boldsymbol{u}_0 - \boldsymbol{u}_s, \tag{3.6a}$$

$$\boldsymbol{u}_\Delta^b := \boldsymbol{u}_\Delta^a - \sum_{i=1}^{N} \left(\boldsymbol{u}_\Delta^a,\ \boldsymbol{u}_i\right)_\Omega \boldsymbol{u}_i, \tag{3.6b}$$

$$\boldsymbol{u}_\Delta := \frac{\boldsymbol{u}_\Delta^b}{\left\|\boldsymbol{u}_\Delta^b\right\|_\Omega}. \tag{3.6c}$$

The field $\boldsymbol{u}_\Delta$ will be called the *shift-mode*, since it represents the 'shift' of the short-term averaged flow away from the Karhunen–Loève space. Figure 7 illustrates the construction of this mode.

This shift-mode can formally be considered as the $(N+1)$th expansion mode $\boldsymbol{u}_{N+1} := \boldsymbol{u}_\Delta$ in a generalized Karhunen–Loève decomposition. By construction, $\{\boldsymbol{u}_i\}_{i=1}^{N+1}$ remains an orthonormal system, i.e. $(\boldsymbol{u}_i, \boldsymbol{u}_j)_\Omega = \delta_{ij}$ for all $i, j = 1, 2, \ldots, N+1$, where δ_{ij} denotes the Kronecker symbol.

Effectively, the shift-mode is a normalized mean-field correction. This correction $\boldsymbol{u}_\Delta^a$ is symmetric with respect to the x-axis and is hence orthogonal to odd-numbered Karhunen–Loève-mode pairs with anti-symmetry, i.e. $\boldsymbol{u}_{1,2}$, $\boldsymbol{u}_{5,6}$, etc. Additionally, $\boldsymbol{u}_\Delta^a$ is nearly orthogonal to the even-numbered mode pairs. These modes can be considered as travelling waves on a slowly varying shift-mode in the downstream direction, i.e. the contributions of two alternating vortices almost annihilate each other. Thus, the remaining Gram–Schmidt corrections, represented by the inner products with $\boldsymbol{u}_{3,4}$, $\boldsymbol{u}_{7,8}$, etc., are the order of 10^{-3}.

The generalized Karhunen–Loève decomposition is expressed by

$$\boldsymbol{u}(\boldsymbol{x}, t) \approx \boldsymbol{u}^{[N+1]} := \sum_{i=0}^{N+1} a_i(t)\, \boldsymbol{u}_i(\boldsymbol{x}), \tag{3.7}$$

where $a_0 := 1$ — following a convention of Rempfer (1991) (see also Rempfer & Fasel 1994*a*, *b*). The Galerkin system is derived from (3.7) with a standard Galerkin projection on the Navier–Stokes equation (3.1*b*). Following Deane *et al.* (1991) and Ma & Karniadakis (2002), the Galerkin projection of the pressure term is found to be negligible. This omission has been justified by validating Galerkin models with and without a pressure term against the direct numerical simulations and by monitoring the neglected pressure term. The Galerkin projection of the remaining acceleration, convection, and dissipation term yields the Galerkin system

$$\frac{\mathrm{d}}{\mathrm{d}t} a_i = \frac{1}{Re} \sum_{j=0}^{N+1} l_{ij} a_j + \sum_{j,k=0}^{N+1} q_{ijk} a_j a_k \quad \text{for} \quad i = 1, \ldots, N+1 \tag{3.8}$$

with coefficients $l_{ij} := (\boldsymbol{u}_i, \Delta \boldsymbol{u}_j)_\Omega$ and $q_{ijk} := (\boldsymbol{u}_i, \nabla \cdot (\boldsymbol{u}_j\, \boldsymbol{u}_k))_\Omega$. The Galerkin approximation (3.7) and the Galerkin system (3.8) constitute the generalized empirical Galerkin model.

3.3. *Invariant-manifold reduction*

In this subsection, the Galerkin system is reduced to the dynamics on an invariant manifold. This reduction exploits the stability characteristics of the cylinder wake. The flow becomes unstable in a supercritical Hopf bifurcation (Sreenivasan, Strykowski & Olinger 1987) and remains governed by an oscillatory instability of the steady solution over the entire laminar shedding regime. The stability spectrum consists

of a single complex-conjugate pair of eigenvalues with positive growth rate whereas the remaining eigenvalues represent strongly damped eigenmodes (Jackson 1987; Zebib 1987; Noack & Eckelmann 1994*b*). The system reduction follows a recipe of synergetics (Haken 1983, § 7) in which the unstable eigenmode is considered as an 'active' degree of freedom while the damped eigenmodes are 'slaved' on an invariant manifold to the active modes.

It may be useful to stress that the proposed reduction deviates, in some aspects, from the standard centre-manifold reduction for the supercritical Hopf bifurcation as described by Guckenheimer & Holmes (1986), and as applied to the cylinder wake by Copeland & Noack (2000). In particular, the Reynolds-number unfolding near the onset of oscillations is sacrificed targeting a more accurate description at the highly supercritical Reynolds numbers. In a similar spirit, only a linear transformation is employed to simplify the Galerkin system. No nonlinear transformation is carried out to reduce the number of nonlinear terms, as in some other centre-manifold studies.

The reduction is performed in five steps:

(i) *Computation of the steady solution* $\boldsymbol{a}_s$ of the Galerkin system (3.8).

(ii) *Linear stability analysis of the steady solution.* A Jordan form decomposition of the linearized Galerkin system (3.8) at $\boldsymbol{a}_s$ yields the eigenmodes $\boldsymbol{\Phi}_i$ with eigenvalues $\sigma_i + \mathrm{i}\omega_i$, where σ_i is the growth rate, ω_i is the circular frequency, and i is the imaginary unit. These eigenmodes are generally not mutually orthogonal. However, they are linearly independent, and form a state-space basis under generic conditions (a non-degenerate spectrum).†

(iii) *Coordinate change via a linear transformation.* The Fourier coefficients can be expressed as a linear expansion with the eigenmodes $\boldsymbol{\Phi}_i$,

$$\boldsymbol{a} = \boldsymbol{a}_s + \sum_{i=1}^{N+1} b_i \boldsymbol{\Phi}_i,$$

and the autonomous system for the normal coordinates b_i has the same form as the original system,

$$\frac{\mathrm{d}}{\mathrm{d}t} b_i = \sum_{j=1}^{N+1} l_{ij}^{\mathrm{NF}} b_j + \sum_{j,k=1}^{N+1} q_{ijk}^{\mathrm{NF}} b_j b_k \quad \text{for} \quad i = 1, 2, \ldots, N+1.$$

The coefficients l_{ij}^{NF} and q_{ijk}^{NF} can be derived from the Galerkin system (3.8). Note that the summation does not include $j = 0$ or $k = 0$ and that $(b_1, b_2, \ldots, b_{N+1}) = \boldsymbol{0}$ is a fixed point by construction.

In compact vector notation, the evolution equation can be expressed by

$$\frac{\mathrm{d}}{\mathrm{d}t} \boldsymbol{b} = \boldsymbol{f}^{\mathrm{NF}}(\boldsymbol{b}),$$

where $\boldsymbol{b} := (b_1, b_2, \ldots, b_{N+1})$ and $\boldsymbol{f}^{\mathrm{NF}}$ summarizes the components of the linear and quadratic term.

(iv) *Invariant-manifold approximation.* This approximation is based on the decomposition of the normal coordinates into two active coordinates

$$\boldsymbol{b}_a = G[\boldsymbol{b}] := (b_1, b_2, 0, \ldots, 0),$$

† In the non-generic case of higher-order eigenvalues, the basis may comprise Jordan chains of generalized eigenvectors, instead of eigenvectors alone.

and the remaining slaved coordinates

$$\boldsymbol{b}_s = H[\boldsymbol{b}] := (0, 0, b_3, \ldots, b_{N+1}).$$

Thus, the active (respectively, slaved) coordinates correspond to unstable (respectively, stable) phase-space directions, similar to the illustrating example of § 2. The slaved coordinates are expressed as functions of the active ones. The lowest non-trivial Taylor expansion of the invariant manifold is given by a quadratic form,

$$b_i = h_{i11} b_1^2 + h_{i12} b_1 b_2 + h_{i22} b_2^2 \quad \text{for} \quad i = 3, \ldots, N+1.$$

The coefficients h_{i11}, h_{i12}, h_{i22} are derived from a consistency condition which minimizes the deviation between the original and reduced system (see for instance Guckenheimer & Holmes 1986, § 3.2, equation 3.2.16). The resulting manifold is denoted by $\boldsymbol{b}_s = \boldsymbol{h}(\boldsymbol{b}_a)$

(v) *Invariant-manifold system.* The resulting two-dimensional system is expressed by

$$\frac{\mathrm{d}}{\mathrm{d}t}\boldsymbol{b}_a = G[\boldsymbol{f}^{\mathrm{NF}}(\boldsymbol{b}_a + \boldsymbol{h}(\boldsymbol{b}_a))].$$

Detailed descriptions can be found in many textbooks and reports (see for instance Guckenheimer & Holmes 1986; Holmes *et al.* 1998; Copeland & Noack 2000). These sources also contain the derivation of the Landau equation from the invariant-manifold model by a nonlinear transformation.

3.4. *Mean-field reduction*

In this subsection, a mean-field ansatz is pursued as a physical system-reduction approach. Physical approaches are based on (intuitive) simplifications of the solution ansatz, whereas mathematical methods aim to derive these simplifications from the full evolution equation and small parameters. The mean-field model provides both an additional context and a justification for a minimal generalized Galerkin model and for the invariant-manifold reduction of the previous subsection.

Following the basic premises of mean-field theory in Stuart (1958, 1971), a Galerkin approximation is constructed with a basic mode $\boldsymbol{u}_0$, with a basis for the oscillatory fluctuation (first harmonic) $\boldsymbol{u}_1$, $\boldsymbol{u}_2$, and with the Reynolds-stress effect of the fluctuation on the mean-field correction $\boldsymbol{u}_\Delta$. The ansatz is represented by

$$\boldsymbol{u} = \boldsymbol{u}_0 + a_1\boldsymbol{u}_1 + a_2\boldsymbol{u}_2 + a_\Delta\boldsymbol{u}_\Delta. \tag{3.9}$$

In mean-field theory, the steady solution is the basic mode $\boldsymbol{u}_0$, the oscillation modes $\boldsymbol{u}_1$, $\boldsymbol{u}_2$ are (essentially) the real and imaginary part of the associated most unstable eigenmode, and the shift-mode $\boldsymbol{u}_\Delta$ is derived from a linearized Reynolds equation. In the present study, the higher harmonics are neglected, as in mean-field theory. In contrast to mean-field theory, the ansatz is considered as a perturbation of the limit cycle as opposed to a perturbation of the steady solution. In this context, the mean flow is taken as the basic mode, the oscillatory modes are the first two Karhunen–Loève modes, and the shift-mode is geometrically constructed from knowledge of the steady solution and averaged flow (see § 3.2).

The dynamics of the Fourier coefficients are derived with a standard Galerkin projection on the Navier–Stokes equation. This projection leads to

$$\frac{\mathrm{d}}{\mathrm{d}t}a_i = \frac{1}{Re}\sum_{j=0}^{3} l_{ij}^{\mathrm{MFM}} a_j + \sum_{j,k=0}^{3} q_{ijk}^{\mathrm{MFM}} a_j a_k \quad \text{for} \quad i = 1, 2, 3, \tag{3.10}$$

where a_Δ is identified with a_3. This system is the generalized Galerkin model with $N = 2$ and will be referred to as the *minimal Galerkin system.*

The minimal Galerkin system is simplified by a Kryloff–Bogoliubov ansatz (see for instance Jordan & Smith 1988) for the oscillatory solution,

$$a_1 = A\ \cos\omega t, \tag{3.11a}$$

$$a_2 = A\ \sin\omega t, \tag{3.11b}$$

$$a_\Delta = B. \tag{3.11c}$$

A minus sign may need to be added on the right-hand side of (3.11*b*) to be consistent with the direction of rotation of the minimal Galerkin system (3.10). In the limit cycle, the shift-mode amplitude vanishes, $B = 0$, and the oscillation amplitude A and frequency ω are constant. In non-equilibrium conditions, B remains relatively small and A, B, and ω are considered as slowly varying functions of time compared to the period of oscillation. Formally, the assumed slow variation can be expressed by $A = A(\epsilon t)$, $B = B(\epsilon t)$, $\omega = \omega(\epsilon t)$, where ϵ is a small parameter.

This parameter will be estimated below from the Landau model (see for instance Landau & Lifshitz 1987, § 26). The equations for the amplitude A and the phase ϕ of the supercritical Hopf bifurcation considered are given by

$$\mathrm{d}A/\mathrm{d}t = \sigma_1 A - \beta A^3, \qquad \mathrm{d}\phi/\mathrm{d}t = \omega_1 + \gamma A^2$$

with the positive growth rate σ_1 and the frequency ω_1 of the most unstable linear stability eigenmode, the positive Landau constant β, and the nonlinearity parameter γ. The Landau model is assumed only to describe the transient phase and no assumptions on the Reynolds-number dependence of the stability eigenvalue $\lambda = \sigma_1 \pm \mathrm{i}\omega_1$ and the nonlinearity parameters β, γ are implied – in complete analogy to the invariant-manifold model. The amplitude and time are normalized to yield a final amplitude and initial frequency of unity. This normalization leads to the amplitude equation

$$\mathrm{d}A/\mathrm{d}t = \alpha\ (A - A^3),$$

where A is the normalized amplitude and $\alpha := \sigma_1/\omega_1$. A linearization around the limit cycle with the Taylor expansion $A = 1 + A' + O(A'^2)$ leads to the first variational form for the amplitude perturbation A',

$$\mathrm{d}A'/\mathrm{d}t = -2\alpha A'.$$

The damping rate $\epsilon := 2\,\alpha = 2\sigma_1/\omega_1$ can be taken as a good *a priori* representation of the small parameter.

According to the Kryloff–Bogoliubov ansatz, the left-hand side of (3.10) at $i = 3$ is of order ϵB and can be neglected. Thus, averaging the third equation of the minimal Galerkin system over one period yields

$$B = B_0 + cA^2, \tag{3.12}$$

where

$$B_0 = -c_0/c_B, \quad c = -c_A/c_B,$$

$$c_0 = q_{300}^{\mathrm{MFM}} + \frac{1}{Re}\, l_{30}^{\mathrm{MFM}}, \quad c_A = \tfrac{1}{2}\left(q_{311}^{\mathrm{MFM}} + q_{322}^{\mathrm{MFM}}\right), \quad c_B = q_{303}^{\mathrm{MFM}} + q_{330}^{\mathrm{MFM}} + \frac{1}{Re} l_{33}^{\mathrm{MFM}}.$$

Equation (3.12) defines a paraboloid in the three-dimensional phase space, a_1, a_2, a_3. This paraboloid is tangent to the (a_1, a_2)-plane at the predicted fixed point $B = B_0$, $A = 0$ and characterizes how the shift-mode amplitude B is slaved to the oscillation

amplitude A. The paraboloid is the analogue of the invariant manifold and depends on the Reynolds number, in contrast to the quadratic invariant-manifold approximation near the Hopf bifurcation. It is worthwhile to note that the invariant-manifold reduction and mean-field model are identical for phase-invariant dynamics of a single harmonic (see Noack & Copeland 2000).

The evolution equation of A is derived from first two equations of the minimal Galerkin system (3.10) as follows. Differentiation of $A^2 = a_1^2 + a_2^2$ with respect to time yields $A\,\mathrm{d}A/\mathrm{d}t = a_1 \mathrm{d}a_1/\mathrm{d}t + a_2 \mathrm{d}a_2/\mathrm{d}t$. Substituting the time derivatives of the Fourier coefficients from (3.10), inserting the Kryloff–Bogoliubov ansatz (3.11*a*, *b*)and averaging over one period yields

$$\frac{\mathrm{d}}{\mathrm{d}t} A = \sigma_B A, \tag{3.13}$$

where

$$\sigma_B = b_0 + b_\Delta B,$$
$$2b_0 = q_{110}^{\mathrm{MFM}} + q_{220}^{\mathrm{MFM}} + q_{101}^{\mathrm{MFM}} + q_{202}^{\mathrm{MFM}} + \frac{1}{Re}\left(l_{11}^{\mathrm{MFM}} + l_{22}^{\mathrm{MFM}}\right),$$
$$2b_\Delta = q_{113}^{\mathrm{MFM}} + q_{223}^{\mathrm{MFM}} + q_{131}^{\mathrm{MFM}} + q_{232}^{\mathrm{MFM}}.$$

We shall not pause to derive the frequency equation and the interested reader is referred to two methods in Noack & Copeland (2000) and Copeland & Noack (2000).

The behaviour of the mean-field model can easily be inferred from the constitutive equations (3.12), (3.13). The fixed point is given by

$$A_s = 0, \quad B_s = B_0. \tag{3.14}$$

The growth rate of the infinitesimal perturbation is defined as (3.13),

$$\sigma_s = b_0 + b_\Delta B_0. \tag{3.15}$$

Hence, the characteristic time for a transient from the fixed point to the limit cycle can be estimated as $1/\sigma_s$. The limit cycle is defined by a vanishing growth of the oscillation amplitude, $\sigma_B = 0$, i.e.

$$A_\infty = \sqrt{\frac{B_\infty - B_0}{c}}, \tag{3.16a}$$

$$B_\infty = -\frac{b_0}{b_\Delta}. \tag{3.16b}$$

The form of the proposed mean-field model (3.9), (3.11), (3.12), (3.13) is consistent with weakly nonlinear theories for the onset of a soft bifurcation. The Landau equation, for instance, is obtained by an elimination of the shift-mode amplitude,

$$\frac{\mathrm{d}}{\mathrm{d}t} A = \sigma_s\, A - \beta A^3, \tag{3.17}$$

with the initial growth rate σ_s and the Landau constant $\beta = -b_0 c$. Similarly, the more general mean-field equations by Stuart (1958) are obtained by a translation of the shift-mode equation.

Note that the mean-field model presented here is derived for a small, non-equilibrium deviation of the limit cycle. *A priori,* the model cannot be expected to describe the transients far away from the limit cycle. In addition, neglecting the higher harmonics can only be justified *a posteriori* based on the simulation results.

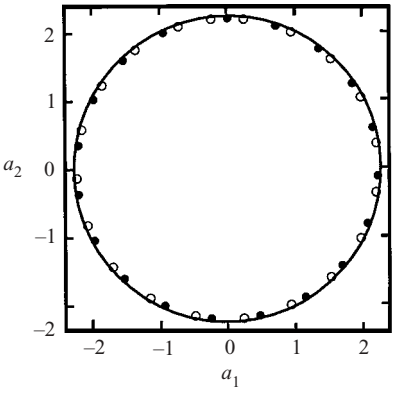

FIGURE 8. Galerkin attractor and Navier–Stokes attractor at $Re = 100$. The first two coefficients $(a_1(t), a_2(t))$ of the periodic Galerkin solution are shown at discrete times. The attractors of Galerkin models A (○) and B (●) are very similar. The solid line represents the direct numerical simulation.

4. Galerkin model

The effect of the shift-mode is the focus of this section. The discussion provides a comparison of *Galerkin model A* without the shift-mode, representing the state-of-the-art benchmark (e.g. following Deane *et al.* 1991), and *Galerkin model B* with the shift-mode. In other words, models A and B are based on the standard Karhunen–Loève decomposition (3.2) and on the generalized decomposition (3.7), respectively. The number of Karhunen–Loève modes is $N = 8$ and the Reynolds number is 100 in agreement with a parameter choice of Deane *et al.* (1991). In § 4.1 and § 4.2, the attractor and associated modal energy-flow cascade are considered. In § 4.3 and § 4.4, the respective transient dynamics and the Reynolds-number dependence are studied.

4.1. *Periodic solution*

Both Galerkin models considered have asymptotically stable limit cycles. The corresponding periodic solutions are shown in figure 8. The Fourier coefficients of the higher modes resolve higher harmonics of the dynamics. This behaviour has already been described by Deane *et al.* (1991) for laminar vortex shedding and by Ma & Karniadakis (2002) for transitional vortex shedding.

The shift-mode amplitude of model B vanishes and the periodic solutions are almost identical. Hence, the generalization for transient behaviour has negligible effect on the attractor. This behaviour is to be expected since the shift-mode is orthogonal to the attractor and its amplitude should vanish by construction. The same conclusions have been reached by Noack, Papas & Monkewitz (2002) in equivalent models of the Kelvin–Helmholtz vortices in a laminar shear layer. Summarizing, the accuracy of Galerkin models A and B is comparable for the periodic solution of the reference simulation where the shift-mode plays no role.

4.2. *Energy-flow analysis*

The modal energy-flow cascade of the periodic flow is particularly useful in the identification of the energetic role of individual modes. A straightforward energy-flow analysis (Rempfer 1991; Noack *et al.* 2002) yields an energy-balance equation for the ith mode. In the following, $\langle\,\rangle$ represents the time average, so that $\boldsymbol{u}_0 = \langle \boldsymbol{u} \rangle$ is the mean flow, and $\boldsymbol{u}' = \boldsymbol{u} - \boldsymbol{u}_0$ is the fluctuation. In addition, the contribution of the ith mode to the production, convection, transfer term, and dissipation are denoted by $\mathscr{P}_i$,

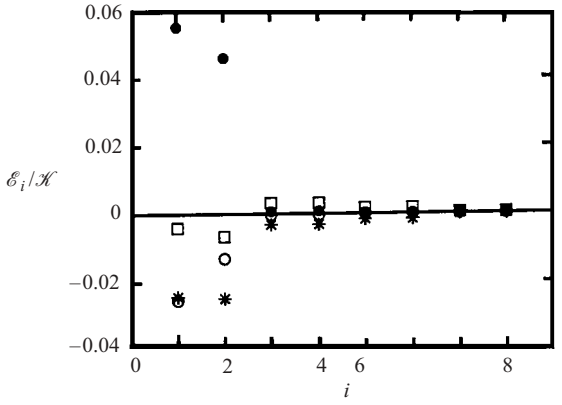

FIGURE 9. Modal energy-flow analysis of the periodic Navier–Stokes solution at $Re = 100$. The modal production $\mathscr{P}_i$ (●), convection $\mathscr{C}_i$ (○), transfer term $\mathscr{T}_i$ (□), and dissipation term $\mathscr{D}_i$ (⋆) from (4.2) are shown as functions of the mode index i. These energy terms are normalized with the total averaged turbulent kinetic energy $\mathscr{K}$. The reciprocal of this normalized value indicates the number of time units to produce or dissipate the energy content of the domain.

$\mathscr{C}_i$, $\mathscr{T}_i$, and $\mathscr{D}_i$, respectively. We neglect the pressure-work term in agreement with the simplified Galerkin projection. The investigation is carried out on the Navier–Stokes attractor, i.e. the properties of the Karhunen–Loève decomposition,

$$\langle a_i \rangle = 0 \quad \text{and} \quad \langle a_i a_j \rangle = \lambda_i \delta_{ij}, \tag{4.1}$$

are employed. Then, the energy-flow balance for the ith mode yields

$$0 = \mathscr{P}_i + \mathscr{C}_i + \mathscr{T}_i + \mathscr{D}_i \tag{4.2}$$

where

$$\mathscr{P}_i = \langle (a_i \, \boldsymbol{u}_i, \, \nabla \cdot [\boldsymbol{u}' \, \boldsymbol{u}_0])_\Omega \rangle,$$
$$\mathscr{C}_i = \langle (a_i \, \boldsymbol{u}_i, \nabla \cdot [\boldsymbol{u}_0 \, \boldsymbol{u}'])_\Omega \rangle,$$
$$\mathscr{T}_i = \langle (a_i \, \boldsymbol{u}_i, \nabla \cdot [\boldsymbol{u}' \, \boldsymbol{u}'])_\Omega \rangle,$$
$$\mathscr{D}_i = \frac{1}{Re} \langle (a_i \, \boldsymbol{u}_i, \, \triangle \boldsymbol{u}')_\Omega \rangle.$$

These terms can easily be expressed in terms of the Fourier coefficients using (3.2), (3.8), (4.1):

$$\mathscr{P}_i = q_{ii0} \, \lambda_i, \tag{4.3a}$$
$$\mathscr{C}_i = q_{i0i} \, \lambda_i, \tag{4.3b}$$
$$\mathscr{T}_i = \sum_{j,k=1}^{N} q_{ijk} \langle a_i a_j a_k \rangle, \tag{4.3c}$$
$$\mathscr{D}_i = \frac{1}{Re} \, l_{ii} \lambda_i. \tag{4.3d}$$

Of course, the equality sign in (4.3c) is correct only in the limit as $N \to \infty$.

Figure 9 displays the modal energy-flow terms. The two von Kármán modes $\boldsymbol{u}_{1,2}$ are responsible for more than 99% of the total production. This energy flow is partially convected out of the domain, partially dissipated by these modes, and partially transferred to higher modes by nonlinearity. The energy flow to modes $\boldsymbol{u}_{3,4}$

is partially dissipated in these modes and partially transferred to modes $\boldsymbol{u}_{5,6}$ via interaction between $\boldsymbol{u}_{1,2}$ and $\boldsymbol{u}_{3,4}$, and so on. This behaviour is reminiscent of the Kolmogorov cascade in which energy flows from the large-scale modes to the small-scale ones (see for instance Landau & Lifshitz 1987, chap. 3). The same behaviour has also been observed by Noack *et al.* (2002) in shear layers and by Rempfer (1991) in transitional boundary layers.

The modal energy-flow cascade represents an amplitude-damping mechanism, i.e. the higher harmonics absorb the excess energy production by modes $\boldsymbol{u}_{1,2}$. If the Galerkin system is truncated too severely, the energy-flow cascade cannot reach the small-scale modes. In this case, the oscillation amplitude is either too large, for instance at $N = 4$, or it explodes at $N = 2$. Thus, the modal energy-flow analysis explains reported truncation errors by Deane *et al.* (1991).

4.3. *Transient solution*

Here, the transient behaviour of Galerkin models A and B is compared with a global linear stability analysis of the steady solution and with a direct numerical simulation.

The fixed point of Galerkin model A is numerically observed to be very close to the origin $\boldsymbol{a}_s \approx 0$. This fixed point corresponds approximately to the averaged flow $\boldsymbol{u}_0$. This prediction is not physical, since the steady solution $\boldsymbol{u}_s$ has, for instance, a much longer vortex bubble than the mean flow $\boldsymbol{u}_0$ (see figure 7). The reason can be traced back to the different spatial properties of the Karhunen–Loève and the mean-flow modes. Substituting $\boldsymbol{a}_s = 0$ in (3.8) yields the terms $Re^{-1} l_{i0} + q_{i00}$ on the right-hand side. Some of these terms vanish for reasons of symmetry and the remaining coefficients, l_{i0}, q_{i00}, are numerically found to be small. From a physical perspective, these coefficients are expected to be small since they represent projections of the mean-flow Navier–Stokes terms $\nu \Delta \boldsymbol{u}_0$ and $-\nabla \cdot (\boldsymbol{u}_0 \boldsymbol{u}_0)$ with a slow streamwise variation onto the nearly orthogonal Karhunen–Loève modes with an oscillatory streamwise behaviour.

Galerkin model B reproduces the steady Navier–Stokes solution $\boldsymbol{u}_s$ as fixed point. This reproduction is not surprising since the generalized Galerkin ansatz (3.7) incorporates the steady Navier–Stokes solution in its phase space by construction and the Galerkin projection preserves the associated fixed-point property. The fixed point in phase space is well-approximated by $\boldsymbol{a}_s = -\|\boldsymbol{u}_0 - \boldsymbol{u}_s\|_\Omega \, \hat{\mathbf{e}}_{N+1}$, where $\hat{\mathbf{e}}_{N+1} := (0, 0, \ldots, 0, 1)$ denotes the unit vector in the shift-mode direction.

Figure 10 displays the transient solution of Galerkin model B from the fixed point to the limit cycle. The Fourier coefficients of the steady and periodic Navier–Stokes solution are displayed in the same figure. The transient is seen to stay near a paraboloid in agreement with the mean-field prediction (see § 3.4). This aspect is investigated later (see § 5). The transient solution of Galerkin model A remains in the $a_\Delta = 0$ plane by construction.

The transient times of Galerkin models A and B are compared with a numerical simulation and a global linear stability analysis in figure 11. The initial condition of the simulation at time $t = 0$ is given by $\boldsymbol{u} = \boldsymbol{u}_s + 0.01\,\boldsymbol{u}_1$. The initial conditions of Galerkin models A and B are the corresponding Galerkin approximations $\boldsymbol{a} = \boldsymbol{a}_s + 0.01\hat{\mathbf{e}}_1$. It should be noted that the fixed points $\boldsymbol{a}_s$ of both Galerkin systems differ by the mean-field correction.

In addition, a global linear stability analysis is carried out in order to elucidate the relationship between the simulation and the most amplified infinitesimal perturbation. The stability analysis predicts that the steady solution $\boldsymbol{u}_s$ of the Navier–Stokes equation is unstable at $Re > 47$ (Jackson 1987; Zebib 1987). The most amplified perturbation $\boldsymbol{u}'$ is described by the first eigenmode $\boldsymbol{f}_1$ and its associated

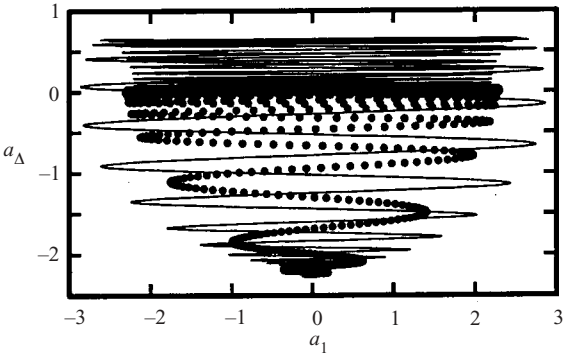

FIGURE 10. Transient solution of the Navier–Stokes equation (solid circles) and Galerkin model B (solid curve). The figure shows $(a_1(t), a_\Delta(t))$ of a transient trajectory starting close to the steady Navier–Stokes solution corresponding to the fixed point in the Galerkin system.

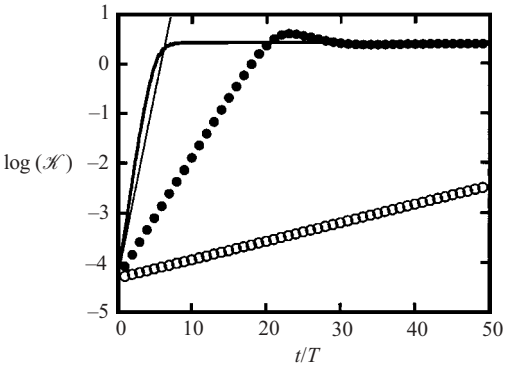

FIGURE 11. Transient solutions of Galerkin model A (○) and B (●). These transients are compared with linear global stability analysis of the Navier–Stokes equation (thin straight line) and the corresponding Navier–Stokes simulation (thick line). The figure displays the turbulent kinetic energy of the fluctuation around the phase-averaged flow in dependency of the time.

complex-conjugate pair of eigenvalues $\sigma_1 \pm \mathrm{i}\omega_1$, where σ_1 represents the growth rate, ω_1 the angular frequency and i the imaginary unit. The fluctuation is expressed by the real part of the normal-mode ansatz $\boldsymbol{u}' = \exp[(\sigma_1 \pm \mathrm{i}\omega_1)\, t]\ \boldsymbol{f}_1(\boldsymbol{x})$. The growth rate of the corresponding turbulent kinetic energy $\mathcal{K}_{\mathrm{LSA}} = (1/2)\, \|\boldsymbol{u}'\|^2_\Omega$ is given by $2\sigma_1$.

The equivalent instantaneous energy quantities of Galerkin models A and B are expressed by $\mathcal{K}_{A,B} = (1/2) \sum_{i=1}^{N} a_i^2$. Note that the shift-mode amplitude a_Δ is not included, since $\boldsymbol{u} = \boldsymbol{u}_s + a_\Delta\, \boldsymbol{u}_\Delta$ is considered as the slowly varying base flow. Figure 11 includes the temporal evolution of the turbulent kinetic energy predicted by linear stability theory, $\mathcal{K}_{\mathrm{LSA}} = 0.00005 \exp[2\sigma_1 t]$, by Galerkin system A, $\mathcal{K}_{\mathrm{A}}$, and by Galerkin system B, $\mathcal{K}_{\mathrm{B}}$. The energy growth of linear stability theory and of the numerical simulation are comparable. However, the transient time of Galerkin system A is more than one hundred shedding periods and thus significantly over-predicted. Galerkin system B is in closer agreement with the numerical simulation. Since the Karhunen–Loève modes and the eigenmodes of the stability analysis are quantitatively quite different (see § 5.4), no exact agreement between the generalized Galerkin system and the stability analysis can be expected.

Galerkin models A and B resolve quite different amplitude-selection mechanisms. The mechanism of model B agrees well with mean-field prediction, i.e. the relative amplitude growth $(\mathrm{d}A/\mathrm{d}t)/A = \sigma_B$ is large near the fixed point and almost vanishes in the limit-cycle plane $a_\Delta = 0$. In contrast, the transient of model A starts in the limit-cycle plane. The initial growth of the turbulent kinetic energy is based on the small excess energy produced by the von Kármán modes $\boldsymbol{u}_{1,2}$. Initially, this energy flow cannot be discharged to the higher harmonics, since the higher harmonics are excited by a nonlinearity close to the saturation.

The strength of the amplitude-selection mechanism is strongly correlated with the robustness of the Galerkin method to small modelling errors. The weak amplitude-selection mechanism of model A with a long transient time scale is physically incorrect and gives rise to a nearly structurally unstable condition. A small modelling error which causes a small additional term in the Galerkin system may also give rise to a Galerkin solution with a large amplitude error, as was illustrated in the context of the motivating example in § 2. In addition, the domain of attraction is limited to a neighbourhood of the limit cycle. In contrast, Galerkin model B has a strong preference towards the limit-cycle amplitude and numerical studies indicate that the limit cycle is globally stable. The mechanism of model B is detailed for the reduced models of § 5.

4.4. *Reynolds-number dependence*

In this subsection, the Reynolds-number dependence of Galerkin models A and B is studied.

Figure 12 displays the oscillation amplitude and Strouhal frequency $St = Df/U$ (f: frequency) of the Galerkin systems and the Navier–Stokes simulations. At the reference Reynolds number, both Galerkin systems reproduce the simulations well. However, the critical Reynolds number of Galerkin system A is 80, far larger than the correct value of 47. With a similar model, Deane *et al.* (1991) also report a Hopf bifurcation near $Re \approx 80$. The amplitude of this system jumps to unrealistically large amplitudes at $Re = 105$. The model of Deane *et al.* (1991) ceases to predict stable oscillations at $Re > 120$. The difference may be related to the significantly larger computational domain which Deane *et al.* employ for their Galerkin model. Finally, the slope of the Strouhal–Reynolds number relationship of Galerkin system A has the wrong sign.

The Reynolds-number variation is more realistically predicted by Galerkin system B with the shift-mode. Galerkin system B accurately predicts the critical Reynolds number of 47 and the amplitude evolution is in good agreement with simulation. The Strouhal number increase with the Reynolds number is qualitatively correctly predicted. Moreover, this system is more robust and less prone to divergent solutions. Indeed, the reproduction of the amplitude–Reynolds number relationship is surprisingly good.

However, not all aspects of Galerkin model B are accurately predicted. For instance, the Strouhal–Reynolds number relationship is only qualitatively correct. The increasing Strouhal number with the Reynolds number is caused by a decrease in the streamwise spacing of the von Kármán vortices. This change of the spatial vortex street structure leads to corresponding changes in the Karhunen–Loève modes. The Karhunen–Loève decomposition at one Reynolds number can resolve only a fraction of the turbulent kinetic energy at another Reynolds number (Deane *et al.* 1991). Nonetheless, Galerkin model B is more robust to these kinds of changes. This robustness is linked to the shift-mode. This mode not only plays a predominant role

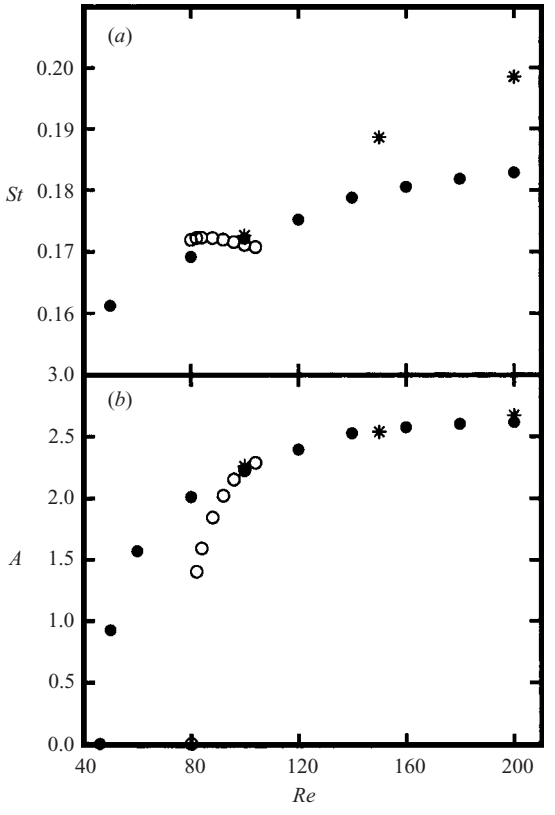

FIGURE 12. Reynolds-number dependence of Galerkin model A (○) and B (●) in comparison with direct numerical simulation (∗): the Strouhal number (*a*) and the amplitude of oscillation $A := \sqrt{\langle a_1^2 + a_2^2 \rangle}$ (*b*).

in the amplitude-selection mechanism, but it also resolves the changes of the steady solution and the averaged flow with the Reynolds number. The shift-mode amplitude a_Δ controls, for instance, the vortex-blob length of the base flow $\boldsymbol{u}_s + a_\Delta \boldsymbol{u}_\Delta$ (see figure 7).

5. Reduced Galerkin models

In this section, three reduced Galerkin models are discussed, the minimal model in § 5.1, the invariant-manifold model in § 5.2, and the mean-field model in § 5.3. All system reductions are based on the generalized Galerkin model B with the shift-mode. The system-reduction possibility without the shift-mode is limited to the minimum mode number of 6 – in agreement with Deane *et al.* (1991). Finally, in § 5.4, the difference between initial and final vortex shedding is assessed in the framework of a global linear stability analysis. This comparison leads to a hybrid model in which the generalized Karhunen–Loève decomposition is enhanced by a stability eigenmode.

5.1. *Minimal Galerkin model*

In this section, the minimal Galerkin model with two Karhunen–Loève modes and the shift-mode is investigated. Figure 13(*a*) displays a transient trajectory from the fixed point to the limit cycle. The trajectory approximately agrees with that of the original

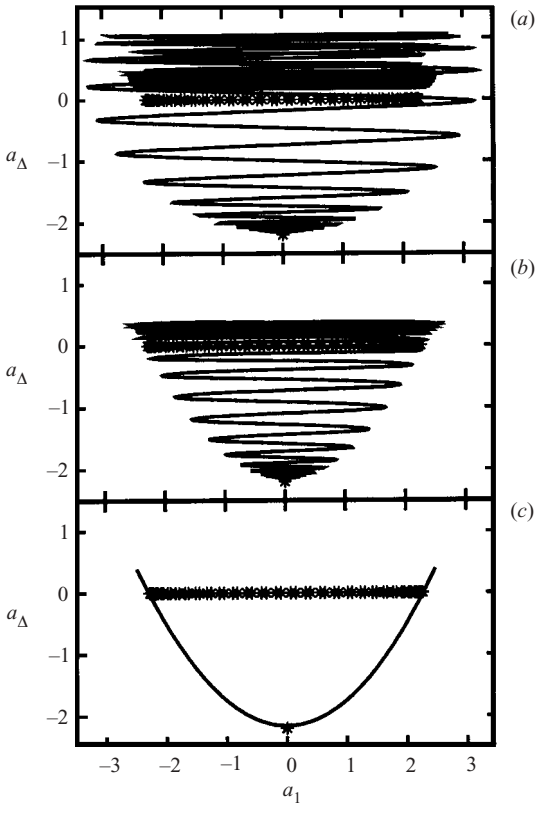

FIGURE 13. Reduced Galerkin models: the minimal 3-mode model (*a*), the invariant-manifold model (*b*), and the mean-field model (*c*). (*a*) and (*b*) show $(a_1(t), a_\Delta(t))$ of a transient trajectory starting close to the fixed point, (*c*) indicates the predicted envelope. The steady and periodic solution of the direct numerical simulation are indicated by stars.

Galerkin model in figure 10. The fixed points of the original and minimal model are virtually identical. However, the oscillation amplitude in the minimal model is 10% too large and the plane of oscillation lies above the $a_\Delta = 0$ plane. This deviation is caused by an interruption of the energy-flow cascade with the neglecting of higher harmonics in the model. Since the modes $\boldsymbol{u}_i$, $i = 3, 4, \ldots$, cannot absorb the excess energy produced by the von Kármán modes $\boldsymbol{u}_{1,2}$, the latter modes grow beyond the correct value until the mean-field deformation $a_\Delta > 0$ can absorb this excess energy via the transfer term. The neglected higher harmonics also lead to the overshoot of the transient on the $a_\Delta > 0$ side of the limit-cycle plane. The damping effect of the higher modes is not resolved in the minimal model.

It may be worthwhile to note that the growth rate of the oscillation amplitude, $\sigma_B = (\mathrm{d}A/\mathrm{d}t)/A$, is nearly a linear function of the distance to the limit-cycle plane $a_\Delta = 0$ – as predicted by mean-field theory in § 3.4. In the limit-cycle plane, $\sigma_B > 0$. Solutions projected in this plane spiral outwards without bound. This explains why a reduced Galerkin model A with $N = 2$ leads to diverging solutions.

5.2. *Invariant-manifold model*

In this subsection, an invariant-manifold reduction of the original Galerkin model B is performed. Figure 13(*b*) displays a transient trajectory from the fixed point to the

periodic solution. The fixed point is not affected by the invariant-manifold reduction. However, the slaving to the invariant manifold prevents the overshoot observed in the original and minimal Galerkin model. The accuracy of the periodic invariant-manifold solution is somewhat better than the mean-field solution. This behaviour can be explained in the framework of the modal energy-flow cascade: The algebraic representation of the invariant manifold is derived from the original model with eight oscillatory modes. As noted earlier, that model resolves the energy flow from the first to higher harmonics. Thus, the excess energy produced by the first harmonics is balanced by the energy-flow cascade. That prediction is qualitatively preserved when the dynamics of higher harmonics is replaced by an algebraic dependence on the leading harmonic in the invariant manifold.

It is worthwhile to note that the shift-mode is the crucial enabler of an invariant-manifold model with an acceptable accuracy. Without the shift-mode, the invariant-manifold model diverges, since the second-order inertial-manifold ansatz can resolve only a small fraction of the energy transfer from the von Kármán modes to the higher modes. However, a higher-order polynomial representation of the invariant manifold can be expected to accommodate a realistic counterpart for Galerkin model B.

5.3. *Mean-field model*

In this subsection, the mean-field model of § 3.4 is studied. Figure 13(*c*) displays the mean-field paraboloid as an envelope of the transient from the fixed point to the periodic solutions. Both the steady and periodic solutions of the model match well with the corresponding solutions of the minimal Galerkin system. The reason for the good agreement rests on the fact that the minimal Galerkin system hardly changes following a rotation around the a_Δ-axis. Thus, the assumed circular limit cycle postulated by the Kryloff–Bogoliubov ansatz (3.11) is consistent with the minimal model. However, the transient a_Δ-overshoot is prevented by the mean-field paraboloid. The 'free' trajectory of the minimal Galerkin system differs noticeably from the 'slaved' mean-field solution. This difference indicates that the ansatz of slowly varying amplitude dynamics is only a coarse approximation. In fact, figure 11 shows that the time scale for the transient dynamics is only one order of magnitude larger than the period of oscillation. In other words, the small parameter ϵ of § 3.4 is approximately 0.3. The relative overshoot of a_Δ compared to the fixed point distance $\|\boldsymbol{a}_s\|$ is also of order ~ 0.1.

5.4. *Linear stability analysis and empirical Galerkin models*

In this subsection, the relationship between the empirical Galerkin models and the global linear stability analysis of the steady solution are studied. This comparison will elucidate the difference between the growth rates of the Navier–Stokes equation and of the model. The study will lead to an augmented Galerkin model. In the following, the Reynolds number is $Re = 100$ for all data considered.

By construction, the Karhunen–Loève decomposition is the optimal basis for the periodic solution with respect to the energy resolution. The first two Karhunen–Loève modes resolve 96% of the total fluctuation energy. However, the oscillatory dynamics associated with the linear instability from the steady solution is only qualitatively represented by the Galerkin model. In contrast, linear stability analysis does provide – again by construction – an accurate basis for the initial part of the transient with its first most unstable complex eigenmode $\boldsymbol{f}_1(\boldsymbol{x})$.

The stability analysis predicts an initial growth rate $\sigma_1 = 0.1439$ and an initial Strouhal number $St_1 = 0.1346$ in good agreement with the simulation. Figure 14(*a*) displays the real part of the first complex eigenmode. The imaginary part is

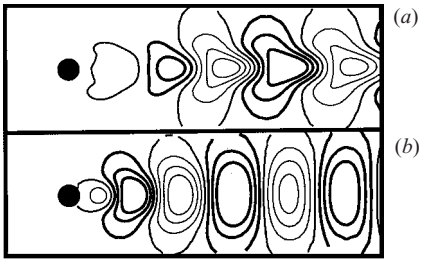

FIGURE 14. Eigenmode of linear stability analysis (*a*) in comparison with the first Karhunen–Loève mode (*b*). The flow field is visualized as in figure 5.

approximately a streamwise phase shift of the real part. This eigenmode is compared with the first Karhunen–Loève mode in figure 14(*b*). Both modes are qualitatively similar and describe an oscillatory wake. However, the characteristic streamwise wavelength of the eigenmode is longer than the corresponding length of the Karhunen–Loève mode. In addition, the initial Strouhal number St_1 is about 21% smaller than its asymptotic value. This inverse relationship between streamwise wake structure and decreased Strouhal number is intuitively obvious and detailed in a phenomenological wake model by Ahlborn, Seto & Noack (2002).

The real and imaginary parts of the first complex eigenmode $\boldsymbol{f}_1(\boldsymbol{x})$ may be employed to construct two expansion modes, $\boldsymbol{u}_1^s$, $\boldsymbol{u}_2^s$. Without loss of generality, these modes are assumed to be orthonormalized. The Galerkin approximation for the fluctuation

$$\boldsymbol{u}' = a_1\boldsymbol{u}_1^s + a_2\boldsymbol{u}_2^s \tag{5.1}$$

resolves – by construction – exactly the initial part of the transient, but only 41% of the turbulent kinetic energy of the periodic vortex shedding. The reason for this low final resolution is clearly illustrated by figure 14: the fluctuation amplitude of the eigenmode is small before the stagnation saddle point of the steady solution (see figure 7*a*) and, thus, hardly resolves the near field dynamics. In contrast, the first two Karhunen–Loève modes describe the vortex shedding also in the near field.

In complete analogy to § 5.1, a three-dimensional Galerkin model is constructed based on the mean flow, the fluctuation (5.1), and a shift-mode $\boldsymbol{u}_\Delta^s$,

$$\boldsymbol{u} = \boldsymbol{u}_0 + a_1\boldsymbol{u}_1^s + a_2\boldsymbol{u}_2^s + a_\Delta\boldsymbol{u}_\Delta^s. \tag{5.2}$$

This shift-mode is obtained from the mean-field correction after the Gram–Schmidt orthonormalization with respect to the new Galerkin ansatz. The shift-modes of this subsection and of § 3.2 are almost identical, since the Karhunen–Loève modes and stability eigenmodes are nearly orthogonal to the steady and averaged flow. In analogy to the generalized Karhunen–Loève ansatz (3.7), all modes of (5.2) are divergence free since stability eigenmodes satisfy the incompressibility condition and the subsequent operations preserve this property.

The minimal Galerkin system is derived in a standard Galerkin projection. This system accurately yields the fixed point as in previous Galerkin models. However, in contrast to the empirical models, the initial growth rate and the frequency are accurately reproduced with an error of less than 1%. The good agreement with the actual growth rates corroborates that the omission of the pressure term in the Galerkin model is also legitimate for the transient dynamics and not only a good approximation for the periodic flow.

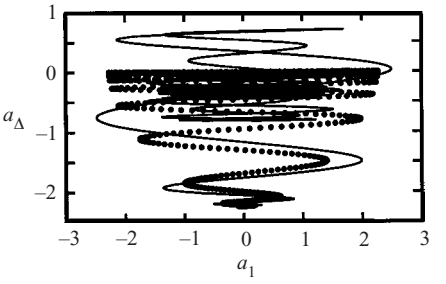

FIGURE 15. Transient solution of the Navier–Stokes equation (●) and the minimal Galerkin model based on the stability eigenmodes of the steady solution (solid curve). The solutions are visualized as in figure 10.

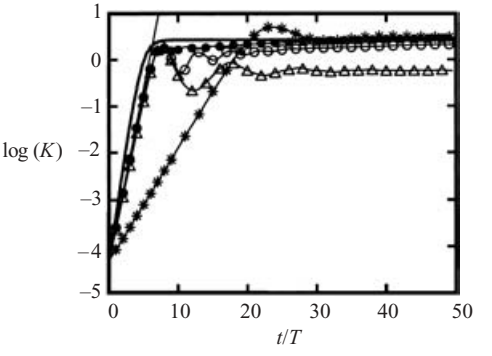

FIGURE 16. As figure 11, but with transient solutions the minimal Galerkin model (⋆), the mean-field model (△), the hybrid model with Karhunen–Loève and stability eigenmodes (○), and the enhanced Galerkin model B (●). The symbols mark the corresponding solid curves.

Figure 15 displays a transient solution from the steady solution to the limit cycle. The growth rate is about three times larger than its counterpart in empirical models. However, in the post-transient limit cycle, the oscillation amplitude is 50% too small and the frequency is 15% too low. The amplitude deviation is of the same order as the unresolved fluctuation energy in the eigenmodes. The oscillation amplitude is too small because the relative resolution of the energy sinks, namely dissipation and convection, with ansatz (5.1) is roughly two times higher than the production as the only energy source. The lower frequency is a direct consequence of a well-defined convection velocity and the over-predicted streamwise wavelength. Despite these quantitative discrepancies, figure 15 demonstrates that the ansatz of a Galerkin model with a shift-mode is surprisingly robust with respect to changes of its expansion modes.

The different shapes of the initial and final wake structures preclude a uniformly accurate minimal Galerkin model for the entire transient from the steady to the periodic solution. Figure 16 displays this compromise in terms of the turbulent kinetic energy. Of the two three-dimensional Galerkin models, the minimal representation employing two Karhunen–Loève modes predicts much better the post-transient fluctuation level whereas the Galerkin model based on (5.2) with the first two stability eigenmodes agrees much better with the transient growth rate.

In order to combine the strengths of the minimal and stability-eigenmode models, a *hybrid model* is constructed with the shift-mode, two Karhunen–Loéve modes, and

two stability eigenmodes. The corresponding Galerkin ansatz is given by

$$\boldsymbol{u} = \boldsymbol{u}_0 + \sum_{i=1}^{2} a_i \boldsymbol{u}_i + a_\Delta \boldsymbol{u}_\Delta + a_1^{s\star} \boldsymbol{u}_1^{s\star} + a_2^{s\star} \boldsymbol{u}_2^{s\star}. \tag{5.3}$$

The two state-space dimensions of the complex stability eigenmode $\boldsymbol{f}_1$ are included in the ansatz (5.3) in analogy to the shift-mode. Here, $\boldsymbol{u}_1^{s\star}$ and $\boldsymbol{u}_2^{s\star}$ are two additional modes, obtained from the respective real and complex parts of $\boldsymbol{f}_1$ after a Gram–Schmidt orthonormalization with respect to $\boldsymbol{u}_1$, $\boldsymbol{u}_2$ and $\boldsymbol{u}_\Delta$. The new modes can be considered as the $(N+2)$th and $(N+3)$th contributions to a further generalization of the Karhunen–Loève decomposition. It may be noted that the order of including new state-space dimensions in the orthonormalization process affects (slightly) the modes and the Fourier coefficients. But this order has no effect on the generalized Karhunen–Loève space and no effect on the velocity fields predicted by the resulting Galerkin model. A change of the order corresponds to an orthonormal coordinate transformation in the Galerkin system.

The hybrid model combines the advantages of both reduced models, i.e. it initially follows the stability analysis and finally converges to the limit cycle (see figure 16). The oscillatory amplitude modulation near the limit cycle is reduced in a higher-dimensional *enhanced Galerkin model B* with one shift-mode, eight Karhunen–Loève modes and two stability eigenmodes (see figure 16). The eigenmodes of this enhanced model are only active during the transient phase like the shift-mode.

6. Conclusions

A simple generalization is proposed for empirical Galerkin models to include transient behaviour. This modification consists of adding a shift-mode so that the Galerkin approximation also includes an accurate representation of the unstable steady solution. For the cylinder wake, the shift-mode leads to the following improvements compared to the Galerkin model based on the Karhunen–Loève decomposition alone:

(i) The steady solution of the Galerkin model is also the steady solution of the Navier–Stokes equation.

(ii) The transient behaviour towards the limit cycle is more realistic. A good match of the growth rates, however, requires the inclusion of the most unstable stability eigenmode.

(iii) The range of validity of the Galerkin model with respect to the Reynolds number is enhanced.

(iv) A potential structural instability of the empirical Galerkin modelling approach is removed.

(v) Mathematical and physical system-reduction approaches lead to a 3-mode model. This model can be further reduced to a mean-field-like model with two degrees of freedom and to a one-dimensional Landau equation for the oscillation amplitude.

(vi) The generalized Galerkin model reveals two important amplitude-selection mechanisms in a single framework. One mechanism is based on the mean-field deformation due to the fluctuation (Stuart 1958). This mechanism is particularly dominant in the neighbourhood of the steady solution. Another process is the energy flow from large-scale modes to smaller-scale ones in the spirit of the Kolmogorov cascade. The role of this process increases with the amplitude of oscillation.

Similar results may be expected for other absolutely unstable flows. The approach presented here has also been applied to an empirical Galerkin model of convectively unstable shear flow. Here, the shift-mode is found to drastically improve the prediction of transient behaviour (Noack *et al.* 2002). The system-reduction capability has been found to be particularly useful for Galerkin-model-based controller design (Gerhard *et al.* 2003).

Often, the required unstable steady solution of the Navier–Stokes equation cannot be computed, for instance in the case of a complex geometry. In this case, one or more additional modes can be computed from a transient simulation. A good choice is expected to be the most energetic orthogonal complement with respect to the Karhunen–Loève decomposition of the attractor. For the cylinder wake, this approach is found to yield nearly identical results. The inclusion of additional modes for non-equilibrium behaviour has been found to be more accurate than the inclusion of transient snapshots for the construction of Karhunen–Loève modes, as suggested by Khibnik *et al.* (2000).

The work has been funded by the Deutsche Forschungsgemeinschaft (DFG) under grant NO 258/1-1 and by the US National Science Foundation (NSF) under grants ECS 0136404, CCR 0208791. The authors acknowledge funding and excellent working conditions of the Collaborative Research Centre (Sfb 557) "Control of complex turbulent flow" which is supported by the DFG and hosted at the Technical University Berlin. Stimulating discussions with Fabio P. Bertolotti, George S. Copeland, Alexander I. Khibnik, Paul Papas, Peter A. Monkewitz, Dietmar Rempfer, Stefan Siegel, and Troy Smith are acknowledged. The low-dimensional modelling and control team at the Technische Universität Berlin – in particular Andreas Dillmann, Rudibert King, Johannes Gerhard, Mandy Goltsch, Mark Pastoor, and Michael Schlegel – has always been a source of valuable advice and inspiration. The authors thank the referees for helpful suggestions.

REFERENCES

Afanasiev, K. 2003 Stabilitätsanalyse, niedrigdimensionale Modellierung und optimale Kontrolle der Kreiszylinderumströmung (transl.: Stability analysis, low-dimensional modelling, and optimal control of the flow around a circular cylinder). PhD thesis, Fakultät Maschinenwesen, Technische Universität Dresden.

Afanasiev, K. & Hinze, M. 2001 Adaptive control of a wake flow using proper orthogonal decomposition. In *Shape Optimization and Optimal Design, Proc. IFIP Conf.* Lecture Notes in Pure and Applied Mathematics, Vol. 216 (ed. J. Cagnol, M. P. Polis & J.-P. Zolesio), pp. 317–332, Marcel Dekker.

Ahlborn, B., Seto, M. L. & Noack, B. R. 2002 On Strouhal number, drag and vortex-street structure. *Fluid Dyn. Res.* **30**, 379–399.

Batcho, P. F. 1994 Gobal spectral methods for the solution of the incompressible Navier–Stokes equations in complex geometries: the generalized Stokes eigensystem. PhD thesis, Princeton University.

Copeland, G.S. & Noack, B. R. 2000 On the Landau equation for vortex shedding. *Tech. Rep.* 02/2000. Hermann-Föttinger-Institut für Strömungsmechanik, Technische Universität Berlin.

Cottet, G. H. & Koumoutsakos, P. 2000 *Vortex Methods – Theory and Practice*. Cambridge University Press.

Deane, A. E., Kevrekidis, I. G., Karniadakis, G. E. & Orszag, S. A. 1991 Low-dimensional models for complex geometry flows: Application to grooved channels and circular cylinders. *Phys. Fluids* A **3**, 2337–2354.

Dušek, J. 1996 Spatial structure of the Bénard von Kármán instability. *Eur. J. Mech.* B/*Fluids* **15**, 619–650.

Dušek, J., Le Gal, P. & Fraunie, P. 1994 A numerical and theoretical study of the first Hopf bifurcation in a cylinder wake. *J. Fluid Mech.* **264**, 59–80.

Fletcher, C. A. J. 1988 *Computational Techniques for Fluid Dynamics. Volume II: Specific Techniques for Different Flow Categories.* Springer.

Föppl, L. 1913 Wirbelbewegung hinter einen Kreiszylinder (transl.: vortex motion behind a circular cylinder) *Sitzb. d. k. bayr. Akad. d. Wiss.* **1**.

Gerhard, J. 2003 Modellbasierter Reglerentwurf zur Unterdrückung der Kármánschen Wirbelstraße im Nachlauf eines umströmten Kreiszylinders anhand niederdimensionaler Galerkin-Modelle (transl.: model-based controller design for the suppression of the von Kármán vortex street in the wake of a circular cylinder in uniform stream employing low-dimensional Galerkin modes). Diplom-thesis, Institut für Prozess- und Anlagentechnik, Technische Universität Berlin.

Gerhard, J., Pastoor, M., King, R., Noack, B. R., Dillmann, A., Morzyński, M. & Tadmor, G. 2003 Model-based control of vortex shedding using low-dimensional Galerkin models. *AIAA Paper* 2003-4262.

Guckenheimer, J. & Holmes, P. 1986 *Nonlinear Oscillations, Dynamical Systems, and Bifurcation of Vector Fields.* Springer.

Haken, H. 1983 *Synergetics, An Introduction. Nonequilibrium Phase Transitions and Self-Organizations in Physics, Chemistry, and Biology, 3rd Edn.* Springer.

Holmes, P., Lumley, J. L. & Berkooz, G. 1998 *Turbulence, Coherent Structures, Dynamical Systems and Symmetry*. Cambridge University Press.

Hu, G.-H., Sun, D.-J., Yin, X.-Y. & Tong, B.-G. 1996 Hopf bifurcation in wakes behind a rotating and translating circular cylinder. *Phys. Fluids* **8**, 1972–1974.

Jackson, C. P. 1987 A finite-element study of the onset of vortex shedding in flow past variously shaped bodies. *J. Fluid Mech.* **182**, 23–45.

Jordan, D. W. & Smith, P. 1988 *Nonlinear Ordinary Differential Equations.* Clarendon.

Karniadakis, G. E. & Triantafyllou, G. S. 1992 Three-dimensional dynamics and transition to turbulence in the wake of bluff bodies. *J. Fluid Mech.* **238**, 1–30.

Kevrekides, Y., Nagia, R. K., Batcho, P. & Karniadakis, G. 1997 Unsteady flows in 2-d complex geometries: bifurcation studies with global eigenfunction expansions. *SIAM J. Sci. Comput.* **18**, 775.

Khibnik, A. I., Narayanan, S., Jacobson, C. A. & Lust, K. 2000 Analysis of low dimensional dynamics of flow separation. In *Continuation Methods in Fluid Dynamics* (ed. D. Henry & A. Bergeon). Notes on Numerical Fluid Mechanics, Vol. 74, pp. 167–178. Vieweg.

Landau, L. D. & Lifshitz, E. M. 1987 *Fluid Mechanics, Course of Theoretical Physics,* Vol. 6. Pergamon.

Ma, X. & Karniadakis, G. E. 2002 A low-dimensional model for simulating three-dimensional cylinder flow. *J. Fluid Mech.* **458**, 181–190.

Morzyński, M. 1987 Numerical solution of Navier–Stokes equations by the finite element method. In *Proc. SYMKOM 87, Compressor and Turbine Stage Flow Path – Theory and Experiment, Lodz, Poland, October 14–16, 1987*, Vol. 3, pp. 119–128.

Morzyński, M., Afanasiev, K. & Thiele, F. 1999 Solution of the eigenvalue problems resulting from global non-parallel flow stability analysis. *Comput. Meth. Appl. Mech. Engng* **169**, 161–176.

Noack, B. R. 1999*a* On the flow around a circular cylinder. Part I: laminar and transitional regime. *Z. Angew. Math. Mech.* **79**, 223–226.

Noack, B. R. 1999*b* On the flow around a circular cylinder. Part II turbulent regime. *Z. Angew. Math. Mech.* **79**, 227–230.

Noack, B. R. & Bertolotti, F. P. 2000 On the stability of turbulent shear flow. In *Intl Workshop on Organized Vortical Motion as a Basis for Boundary-Layer Control, Kiev, Ukraine, September 20–22, 2000* (ed. V. Grinchenko, N. Yurchenko & W. Criminale).

Noack, B. R. & Copeland, G. S. 2000 On a stability property of ensemble-averaged flow. *Tech. Rep.* 03/2000. Hermann-Föttinger-Institut für Strömungsmechanik, Technische Universität Berlin.

Noack, B. R. & Eckelmann, H. 1994*a* A low-dimensional Galerkin method for the three-dimensional flow around a circular cylinder. *Phys. Fluids* **6**, 124–143.

Noack, B. R. & Eckelmann, H. 1994*b* A global stability analysis of the steady and periodic cylinder wake. *J. Fluid Mech.* **270**, 297–330.

Noack, B. R., Papas, P. & Monkewitz, P. A. 2002 Low-dimensional Galerkin model of a laminar shear-layer. *Tech. Rep*. 2002-01. Laboratoire de Mecanique des Fluides, Departement de Genie Mecanique, Ecole Polytechnique Fédérale de Lausanne, Switzerland.

Rempfer, D. 1991 Kohärente Strukturen und Chaos beim laminar-turbulenten Grenzschichtumschlag (transl.: Coherent structures and chaos of the laminar-turbulent boundary-layer transition). PhD thesis, Fakultät Verfahrenstechnik der Universität Stuttgart (Parts of this PhD thesis are published by Rempfer, D. & Fasel, F. H. 1994 in *J. Fluid Mech.* **260** & **275**).

Rempfer, D. 2000 On low-dimensional Galerkin models for fluid flow. *Theor. Comput. Fluid Dyn.* **14**, 75–88.

Rempfer, D. 2003 Low-dimensional modeling and numerical simulation of transition in simple shear flow. *Annu. Rev. Fluid Mech.* **35**, 229–265.

Rempfer, D. & Fasel, F. H. 1994*a* Evolution of three-dimensional coherent structures in a flat-plate boundary layer. *J. Fluid Mech.* **260**, 351–375.

Rempfer, D. & Fasel, F. H. 1994*b* Dynamics of three-dimensional coherent structures in a flat-plate boundary layer. *J. Fluid Mech.* **275**, 257–283.

Rempfer, D., Parsons, L., Xu, S. & Lumley, J. L. 2003 Theoretical approaches to the effect of wall compliance on turbulent flow. In *Proc. IUTAM Symp. on Flow in Collapsible Tubes and Past Other Highly Compliant Boundaries* (ed. P. Carpenter & T. Pedley), pp. 231–252. Kluwer.

Rummler, B. 2000 Zur Lösung der instationären inkompressiblen Navier-Stokesschen Gleichungen in speziellen Gebieten (transl.: On the solution of the incompressible Navier-Stokes equations in some domains). Habilitation thesis, Fakultät für Mathematik, Otto-von-Guericke-Universität Magdeburg.

Sato, H. 1960 The stability and transition of a two-dimensional jet. *J. Fluid Mech.* **7**, 53–80.

Sreenivasan, K. R., Strykowski, P. J. & Olinger, D. J. 1987 Hopf bifurcation, Landau equation, and vortex shedding behind circular cylinders. In *Forum on Unsteady Flow Separation* (ed. K. N. Ghia). American Society for Mechanical Engineers, Fluids Engineering Division, Vol. 52, pp. 1–13.

Stuart, J. T. 1958 On the non-linear mechanics of hydrodynamic stability. *J. Fluid Mech.* **4**, 1–21.

Stuart, J. T. 1971 Nonlinear stability theory. *Annu. Rev. Fluid Mech.* **3**, 347–370.

Tang, S. & Aubry, N. 2000 Suppression of vortex shedding inspired by a low-dimensional model. *J. Fluids Struct.* **14**, 443–468.

Williamson, C. H. K. 1996 Vortex dynamics in the cylinder wake. *Annu. Rev. Fluid Mech.* **28**, 477–539.

Zebib, A. 1987 Stability of viscous flow past a circular cylinder. *J. Engng Maths* **21**, 155–165.

Zhang, H.-Q., Fey, U., Noack, B. R., König, M. & Eckelmann, H. 1995 On the transition of the cylinder wake. *Phys. Fluids* **7**, 779–795.